ORIGINAL ARTICLE

IDH-wildtype glioblastomas and grade III/IV IDH-mutant gliomas show elevated tracer uptake in fibroblast activation protein–specific PET/CT

Manuel Röhrich[1,2] [iD] · Anastasia Loktev[1] · Annika K. Wefers[3,4] · Annette Altmann[1,2] · Daniel Paech[5] ·
Sebastian Adeberg[6] · Paul Windisch[6] · Thomas Hielscher[7] · Paul Flechsig[1] · Ralf Floca[8] · Dominik Leitz[9] ·
Julius P. Schuster[6,10] · Peter E. Huber[6,10] · Jürgen Debus[6] · Andreas von Deimling[3,4] · Thomas Lindner[1] ·
Uwe Haberkorn[1,2,9]

Abstract

Purpose Targeting fibroblast activation protein (FAP) is a new diagnostic approach allowing the visualization of tumor stroma. Here, we applied FAP-specific PET imaging to gliomas. We analyzed the target affinity and specificity of two FAP ligands (FAPI-02 and FAPI-04) in vitro, and the pharmacokinetics and biodistribution in mice in vivo. Clinically, we used ^{68}Ga-labeled FAPI-02/04 for PET imaging in 18 glioma patients (five IDH-mutant gliomas, 13 IDH-wildtype glioblastomas).

Methods For binding studies with ^{177}Lu-radiolabeled FAPI-02/04, we used the glioblastoma cell line U87MG, FAP-transfected fibrosarcoma cells, and CD26-transfected human embryonic kidney cells. For pharmacokinetic and biodistribution studies, U87MG-xenografted mice were injected with ^{68}Ga-labeled compounds followed by small-animal PET imaging and ^{177}Lu-labeled FAPI-02/04, respectively. Clinical PET/CT scans were performed 30 min post intravenous administration of ^{68}Ga-FAPI-02/04. PET and MRI scans were co-registered. Immunohistochemistry was done on 14 gliomas using a FAP-specific antibody.

Results FAPI-02 and FAPI-04 showed high binding specificity to FAP. FAPI-04 demonstrated higher tumor accumulation and delayed elimination compared with FAPI-02 in preclinical studies. IDH-wildtype glioblastomas and grade III/IV, but not grade II, IDH-mutant gliomas showed elevated tracer uptake. In glioblastomas, we observed spots with increased uptake in projection on

---

Manuel Röhrich, Anastasia Loktev, Thomas Lindner, and Uwe Haberkorn are co-authors.

This article is part of the Topical Collection on Oncology – Brain

---

✉ Manuel Röhrich
  manuel.roehrich@med.uni-heidelberg.de

1 Clinical Cooperation Unit Nuclear Medicine, German Cancer Research Center (DKFZ), Im Neuenheimer Feld 400, 69120 Heidelberg, Germany

2 Department of Nuclear Medicine, University Hospital Heidelberg, Heidelberg, Germany

3 Department of Neuropathology, Institute of Pathology, University Hospital Heidelberg, Heidelberg, Germany

4 Clinical Cooperation Unit Neuropathology, German Consortium for Translational Cancer Research (DKTK), German Cancer Research Center (DKFZ), Heidelberg, Germany

5 Division of Radiology, German Cancer Research Center (DKFZ), Heidelberg, Germany

6 Department of Radiation Oncology, University Hospital Heidelberg, Heidelberg, Germany

7 Department of Biostatistics, German Cancer Research Center (DKFZ), Heidelberg, Germany

8 Division of Medical Image Computing, German Cancer Research Center (DKFZ), Heidelberg, Germany

9 Translational Lung Research Center Heidelberg (TLRC), German Center for Lung Research (DZL), Heidelberg, Germany

10 Clinical Cooperation Unit Molecular Radiooncology, German Cancer Research Center (DKFZ), Heidelberg, Germany

contrast-enhancing areas. Immunohistochemistry showed FAP-positive cells with mainly elongated cell bodies and perivascular FAP-positive cells in glioblastomas and an anaplastic IDH-mutant astrocytoma.

Conclusions Using FAP-specific PET imaging, increased tracer uptake in IDH-wildtype glioblastomas and high-grade IDH-mutant astrocytomas, but not in diffuse astrocytomas, may allow non-invasive distinction between low-grade IDH-mutant and high-grade gliomas. Therefore, FAP-specific imaging in gliomas may be useful for follow-up studies although further clinical evaluation is required.

Keywords Glioma · Glioblastoma · FAP · PET · MRI

Introduction

Cancer-associated fibroblasts (CAFs) are now recognized as cells influencing tumor growth, migration, and progression [1–3]. Since CAFs can be found in high amounts in many tumor entities such as breast cancer, colon cancer, and pancreatic cancer, they are in the focus of new antitumor therapies [4]. CAFs are distinguished from normal fibroblasts by the enhanced expression of different genes such as α-smooth muscle actin, fibroblast-specific protein 1, and fibroblast activation protein (FAP) [4–6]. Especially FAP, a type II membrane-bound glycoprotein with dipeptidyl peptidase and endopeptidase activity, can be considered as a promising tumor target [4].

With the objective of selectively targeting FAP-positive tumors, several FAP-specific small molecules were developed based on FAP-specific inhibitors. In previous publications, we demonstrated that these compounds rapidly accumulate in FAP-expressing tumor xenografts as well as in cancer patients [7, 8]. Of a total of 15 compounds, FAPI-02 and FAPI-04 showed the most favorable pharmacokinetics in vivo and were, therefore, selected for further characterization in different tumor entities.

Here, we applied FAP-targeted imaging to gliomas, the most common primary intracranial tumors. According to the World Health Organization (WHO) classification of 2016, gliomas are subdivided into isocitrate dehydrogenase (IDH)–wildtype (wt) gliomas WHO grade I–IV and IDH-mutant (mut) gliomas WHO grade II–IV. The most frequent WHO grade IV gliomas are IDH-wildtype glioblastomas. IDH-mutant gliomas frequently undergo malignant transformation to higher WHO grades [9]. The standard imaging modality for gliomas is magnetic resonance imaging (MRI). In special clinical situations, like biopsy planning or differentiation between tumor progression and radiation necrosis, dynamic positron emission tomography (PET) imaging is added to MRI. For PET imaging of gliomas, radioactive-labeled amino acids like O-(2-[18F]-fluoroethyl)-L-tyrosine (FET) [10], [11C]-methyl-L-methionine (MET) [11, 12], or L-3,4-dihydroxy-6-[18F]-fluorophenylalanine (FDOPA) [13, 14] are used in order to characterize the amino acid uptake of a lesion. FAP-targeted PET imaging delivers complementary information to these modalities by identifying areas with increased stromal activation. Previous histopathological studies showed increased FAP expression in glioblastomas, especially in the mesenchymal subtype [15], and demonstrated that FAP facilitates parenchymal invasion and epithelial to mesenchymal transition of glioblastomas [16]. In this work, FAPI-02 and FAPI-04 were initially evaluated for specific binding and affinity to a glioblastoma cell line in vitro. Thereafter, we performed FAP-specific PET imaging preclinically in a subcutaneous mouse model and clinically in 18 glioma patients to characterize the uptake of FAP ligands in IDH-mutant and IDH-wildtype gliomas.

Materials and methods

Compound synthesis and radiolabeling

FAPI-02 and FAPI-04 were synthesized and radiolabeled with ^{177}Lu and ^{68}Ga according to Loktev et al. [7] and Lindner et al. [8]. Stability in human serum was determined by precipitation of samples and radiochromatographic analysis of the supernatant [8]. Detailed information on compound synthesis and radiolabeling is given in the supplementary information.

In vitro characterization of FAPI-02 and FAPI-04

Radioligand binding studies were performed using the human glioblastoma cell line U87MG (purchased from ATCC, Manassas, USA), FAP-transfected human fibrosarcoma cells (HT-1080-FAP), and CD26-transfected human embryonic kidney cells (HEK-CD26), obtained from Stefan Bauer, NCT Heidelberg. To determine target affinity and specificity of FAPI-02 and FAPI-04, the different cell lines were incubated with the radiolabeled compounds for 60 min at 37 °C, washed twice, and subsequently lysed with lysis buffer (0.2% SDS in 0.3 M NaOH). The radioactivity was measured using a γ-counter, normalized to 1 mio cells, and calculated as percentage of applied dose (%ID/1 mio cells) (for more information on cell culture and assay performance, see supplementary information).

Animal studies

For in vivo experiments, 8-week-old, female BALB/c *nu/nu* mice (Charles River, Wilmington, USA) were subcutaneously inoculated with 5 mio U87MG cells per animal. When the size of the tumor reached approximately 1 cm^3, the radiolabeled compound was injected via the tail vein. PET imaging was performed up to 140 min after intravenous injection of ^{68}Ga-FAPI-02 or ^{68}Ga-FAPI-04 (10 MBq; 80 nmol/GBq) using an Inveon PET small-animal PET scanner (Siemens, Berlin and Munich, Germany). Images were reconstructed iteratively using the 3D ordered subset expectation maximization (OSEM) + maximum a posteriori (MAP) method and were converted to standardized uptake value (SUV) images. Quantification was done using a region of interest (ROI) technique and expressed as mean standardized uptake value. For organ distribution of FAPI-02 and FAPI-04, the animals ($n = 3$ for each time point) were sacrificed 1 h, 4 h, and 24 h after administration of the ^{177}Lu-labeled compound (1 MBq; 200 nmol/GBq). The distributed radioactivity was measured in all dissected organs and in blood using a γ-counter (Cobra Autogamma, Packard, Palo Alto, USA). The values are expressed as percentage of injected dose per gram of tissue (%ID/g).

Immunohistochemistry of xenograft tumors

Unstained and hydrated paraffin sections were pretreated with antigen retrieval solution (Biogenex; 10× Antigen Retrieval Citra Plus) and incubated with 1.5% normal goat serum. Tissue sections were incubated for 1.5 h at 37 °C with a rabbit anti-FAP antibody (Abcam; #ab53066). Secondary biotinylated anti-rabbit antibody was added at a dilution of 1:200 and immunoreactivity was visualized using a peroxidase system (Vector Elite ABC Peroxidase Kit; Vector Laboratories Inc.) together with a 3,39-diaminobenzidine substrate kit (DCS Innovative Diagnostik-Systeme, Hamburg, Germany). Specific binding of the antibody was ensured using negative controls.

Patient characterization

PET/CT scans were applied to 18 glioma patients (aged from 20 to 86 years, average 54.83 years) and analyzed retrospectively. Patients were selected for FAP-specific PET imaging based on the following criteria: (1) adult patients (aged 18 years or older), (2) patients suffering from histologically confirmed gliomas with known IDH status, (3) either treatment-naive patients or patients without treatment within the last 8 weeks before imaging. All diagnoses were proven by stereotaxic biopsy or incomplete resection and histological and molecular (IDH status) diagnosis before imaging. 13 patients suffered from IDH-wildtype glioblastoma WHO grade IV, five patients from IDH-mutant glioma (three WHO grade II, one WHO grade III, one WHO grade IV). Three patients had undergone radiochemotherapy before imaging, two patients chemotherapy. Detailed clinical and pathological patient characteristics are given in Table 1.

Clinical PET/CT imaging

Diagnostic imaging was performed under the conditions of the updated declaration of Helsinki, § 37 (unproven interventions in clinical practice) and in accordance with the German Pharmaceuticals Law §13 (2b) for medical reasons using ^{68}Ga-FAPI-02 (2 patients) and FAPI-04 (16 patients), which was applied intravenously (200 ± 50 MBq), 10 min, 1 h, and 3 h post tracer administration in two patients examined with FAPI-02 and 30 min after tracer administration in the other 16 patients examined with FAPI-04.

The PET/CT scans were performed with a Biograph mCT Flow™ PET/CT-Scanner (Siemens Medical Solutions, Berlin and Munich, Germany) using the following parameters: slice thickness of 5 mm, increment of 3–4 mm, soft tissue reconstruction kernel, care dose. Immediately after CT scanning, a whole-body PET was acquired in 3D (matrix 200 × 200) in FlowMotion™ with 0.7 cm/min. The emission data were corrected for random, scatter, and decay. Reconstruction was conducted with an OSEM algorithm with two iterations/21 subsets and Gauss-filtered to a transaxial resolution of 5 mm at full-width half-maximum. Attenuation correction was performed using the low-dose non-enhanced CT data. The quantitative assessment of standardized uptake values (SUV) was done using a ROI technique. SUV values were corrected for healthy-appearing contralateral brain parenchyma as background (SUV/BG). The imaging protocol was approved by the Institutional Review Board (study number S-016/2018) and conducted according to the guidelines of the Institutional Review Board and to good clinical practice.

Co-registration of PET/CT and MRI scans

For all patients, a corresponding MRI scan for the FAP-specific PET/CT scan (maximum 28 days, average 11.9 days before PET/CT, no change of treatment between the examinations) was available. A post-process co-registration using a MatchPoint [17] based multi modal rigid matching algorithm of contrast-enhanced T1-weighted and T2w/FLAIR sequences with FAP-specific PET scans was carried out with the software Medical Imaging Interaction Toolkit (MITK) Workbench [18].

Immunohistochemistry on human glioma tissue

Immunohistochemistry with a FAP-specific antibody was done on tumors of patients after FAP-specific PET when

Table 1 Clinical data, IDH mutation status, and diagnosis of 18 glioma patients

Patient number	Age (years)	IDH status	Diagnosis	WHO grade	Localization	Biopsy/surgery	Pretreatment
1	57	Wildtype	Glioblastoma	IV	Parietal right	Biopsy	Radiochemotherapy
2	65	Wildtype	Glioblastoma	IV	Bifrontal	Biopsy	None
3	66	Wildtype	Glioblastoma	IV	Parieto-temporal left	Biopsy	None
4	64	Wildtype	Glioblastoma	IV	Temporal right	Resection	Radiochemotherapy
5	58	Wildtype	Glioblastoma	IV	Splenium	Biopsy	None
6	48	wildtype	Glioblastoma	IV	Fronto-temporo-parietal left	Resection	Radiochemotherapy
7	20	Wildtype	Glioblastoma	IV	Thalamus/temporal right	Biopsy	None
8	54	Wildtype	Glioblastoma	IV	Temporal left	Resection	None
9	56	Wildtype	Glioblastoma	IV	Basal ganglia	Partial Resection	None
10	61	Wildtype	Glioblastoma	IV	Temporal right	Resection	None
11	86	Wildtype	Glioblastoma	IV	Corona radiata left	Biopsy	Chemotherapy
12	68	Wildtype	Glioblastoma	IV	Corpus callusom	Biopsy	None
13	71	Wildtype	Glioblastoma	IV	Temporal left	Biopsy	None
14	29	IDH1 R132H mutation	Glioblastoma	IV	Temporo-parietal right	Resection	None
15	47	IDH1 R132H mutation	Anaplastic astrocytoma	III	Frontal right	Resection	None
16	47	IDH1 R132H mutation	Diffuse astrocytoma	II	Parietal left	Biopsy	None
17	47	IDH1 R132C mutation	Diffuse astrocytoma	II	Frontal right	Resection	None
18	43	IDH1 R132H mutation	Diffuse astrocytoma	II	Fronto-temporal left	Biopsy	Chemotherapy

sufficient biopsy material was available. In total, nine IDH-wildtype glioblastomas and all five IDH-mutant gliomas were analyzed. All specimens were from the archives of the Department of Neuropathology, Institute of Pathology, University Hospital Heidelberg, Germany.

The primary anti-FAP antibody used was ab207178 (EPR20021; Abcam, Cambridge, UK) diluted 1:100. Immunohistochemistry was done on 0.5-μm-thick formalin-fixed, paraffin-embedded (FFPE) tissue sections mounted on Superfrost Plus slides (Thermo Scientific, Waltham, MA, USA) followed by drying at 80 °C for 10 min. Stainings were done on a Ventana BenchMark XT Immunostainer (Ventana Medical Systems, Tucson, AZ, USA). The slices were pretreated with cell conditioner 1 (pH 8) for 92 min, followed by incubation with the primary antibody at 37 °C for 32 min. The incubation was followed by Ventana standard signal amplification, UltraWash, counterstaining with one drop of hematoxylin for 4 min and one drop of bluing reagent for 4 min. For visualization, the ultraView™ Universal DAB Detection Kit (Ventana Medical Systems, Tucson, AZ, USA) was used. Negative controls were obtained by omitting the primary antibody (data not shown). Images were taken with an Olympus BX51 microscope (Olympus Deutschland GmbH, Hamburg, Germany).

Statistical analysis

All numerical results are expressed as mean value ± standard deviation (SD). For the SUVmax/BG values, ROC curves and corresponding area under the curve (AUC) estimates including 95% confidence intervals were computed. The analysis was carried out with statistical software R 3.4 [19] using the add-on package "pROC" [20].

Results

In vitro characterization of FAPI-02 and FAPI-04

To evaluate target affinity and specificity of FAPI-02 and FAPI-04, radioligand binding studies were performed using the human glioblastoma cell line U87MG as well as cell lines expressing human FAP and the closely related membrane protein CD26 (52% identity and 71% similarity with high structural resemblance) [21]. As shown in Supplementary Fig. 1, both FAPI-02 and FAPI-04 show robust binding to the FAP-expressing HT-1080 cells after 60 min of incubation (FAPI-02 10.49 ± 0.43, FAPI-04 9.40 ± 0.45 %ID/1 mio cells). In contrast, there is no significant binding to CD26-positive cells (FAPI-02 0.13 ± 0.01, FAPI-04 0.04 %ID/1 mio cells).

These results demonstrate a high binding specificity of the FAPI compounds to its target structure FAP with no affinity to the closely related protein CD26 or different membrane-bound cell proteins. It is, therefore, not surprising that no substantial binding to U87MG cells is detected (FAPI-02 0.52 ± 0.04, FAPI-04 0.37 ± 0.04 %ID/1 mio cells), as this cell line shows no FAP expression in Western blot (suppl. Fig. 1b).

Animal studies

To characterize the pharmacokinetics of FAPI-02 and FAPI-04 in vivo, U87MG-xenografted nude mice were injected with the ^{68}Ga-labeled compounds (80 nmol/GBq) and analyzed by small-animal PET imaging. As shown in Fig. 1a, the radio-tracer gets rapidly enriched within the U87MG tumor, resulting in a strong tumor signal in the first 20 min already (SUV mean 0.63 (FAPI-02) and 1.01 (FAPI-04) after 20 min). While the overall activity is steadily cleared from the bloodstream and excreted through the renal system, tumor activity of FAPI-02 continuously increases (SUV mean 0.67 after 60 min) and is maintained for at least 140 min while the tumor activity of FAPI-04 shows a peak after 4 min (SUV mean 1.24) and then slowly decreases (SUV mean 0.68 after 60 min) (Fig. 1b). Unspecific binding to non-malignant tissues is negligibly low for both tracers, resulting in a low background and high contrast images.

These observations were confirmed in a biodistribution study using ^{177}Lu-labeled FAPI-02 (200 nmol/GBq; Fig. 1c). Again, the radioligand highly accumulates in the U87MG tumor while showing only insignificant activities in blood and all investigated organs. However, FAPI-02 gets also continuously cleared from the tumor tissue with uptake values decreasing from 9.69 ± 1.34 %ID/g after 1 h to 0.88 ± 0.02 %ID/g after 24 h.

As illustrated in Fig. 1c, FAPI-04 shows a significantly higher tumor accumulation than FAPI-02 (29.76 ± 6.99 %ID/g after 1 h) and gets eliminated considerably slower. In contrast to FAPI-02, of which only 9% of the initial activity remains after 24 h, still 18% of the initial activity of FAPI-04 are detectable after 24 h (5.43 ± 0.59 %ID/g). Moreover, FAPI-04 shows even less unspecific binding to non-cancerous tissues than FAPI-02, resulting in overall better tumor-to-organ ratios (Supplementary Fig. 2).

FAP immunohistochemistry of the xenograft tumors showed variably positive areas in the tumors (Fig. 1d). In FAP-positive areas, we observed tightly packed FAP-positive cells (Fig. 1e).

Clinical PET/CT imaging

In two patients with IDH-wildtype GBM, we performed PET scans using FAPI-02 at three different time points (10 min, 1 h, and 3 h after tracer administration). We observed a

tendency towards slightly decreased FAP-specific tracer uptake over time in these patients (patient 2: SUVmax 5.86 after 10 min, 5.73 after 1 h, and 4.95 after 3 h; patient 5: SUVmax 2.03 after 10 min, 1.74 after 1 h, and 1.53 after 3 h). For these two cases, SUVmax values and BG values after 1 h were used for statistical analysis together with the values after 30 min of the other cases in order not to over-estimate tracer uptake. IDH-wildtype glioblastomas showed marked tracer uptake (average SUVmax 4.21 ± 2.38, Fig. 2a,b) and high SUVmax/BG values (average 22.38 ± 12.33, Fig. 2e) due to very low tracer uptake in healthy brain parenchyma (average SUVmax 0.21 ± 0.09). In contrast, diffuse astrocytomas, IDH-mutant, WHO grade II showed only slightly elevated tracer uptake (average SUVmax 0.35 ± 0.10, Fig. 2a,b) and low SUVmax/BG values (average 1.81 ± 0.47, Fig. 2g). IDH-mutant gliomas WHO grade III and IV, e.g., anaplastic astrocytomas and glioblastomas, showed markedly increased uptake (SUVmax 3.4 and 2.2, Fig. 2a,b) and SUVmax/BG values (3.3 and 6.5). SUVmax, BG, and SUVmax/BG values for each tumor are shown in supplementary table 1.

Box plots and ROC curves calculated for SUVmax/BG values showed high sensitivity and specificity for the discrimination of GBM versus non-GBM (AUC 0.964) (Fig. 2c,d) and of IDH-wildtype glioblastomas versus all IDH-mutant gliomas (AUC 0.985) (Fig. 2e,f) and even a 100% discrimination without overlap for WHO grade II versus WHO grade III/IV (AUC 1.0) (Fig. 2g,h).

Correlation of FAPI imaging and MRI morphology

All IDH-wildtype glioblastomas and the IDH-mutant gliomas WHO grade III/IV, but none of the IDH-mutant astrocytomas WHO grade II, showed contrast enhancement in MRI. In the co-registered FAPI-PET/CT and MRI scans, we observed spots with markedly increased tracer uptake adjacent to or within areas with low or missing uptake in projection on the contrast-enhancing and T2w/FLAIR-elevated areas of glioblastomas and IDH-mutant gliomas WHO grade III/IV (Fig. 2a). IDH-mutant gliomas WHO grade II showed a homogenously low tracer uptake in projection on their T2w/FLAIR lesions (Fig. 2a).

Immunohistochemistry shows FAP-positive cells in high-grade gliomas

Paraffin-embedded tissue was available from 14 patients. No IDH-mutant glioma WHO grade II showed any FAP positivity. All IDH-wildtype glioblastomas and IDH-mutant gliomas WHO grade III/IV had FAP-positive areas to a variable extent. In the FAP-positive areas, we observed two patterns of FAP-positive cells (Fig. 3). First, we observed spindle-shaped FAP-positive cells with a fibroblast-like morphology dispersed
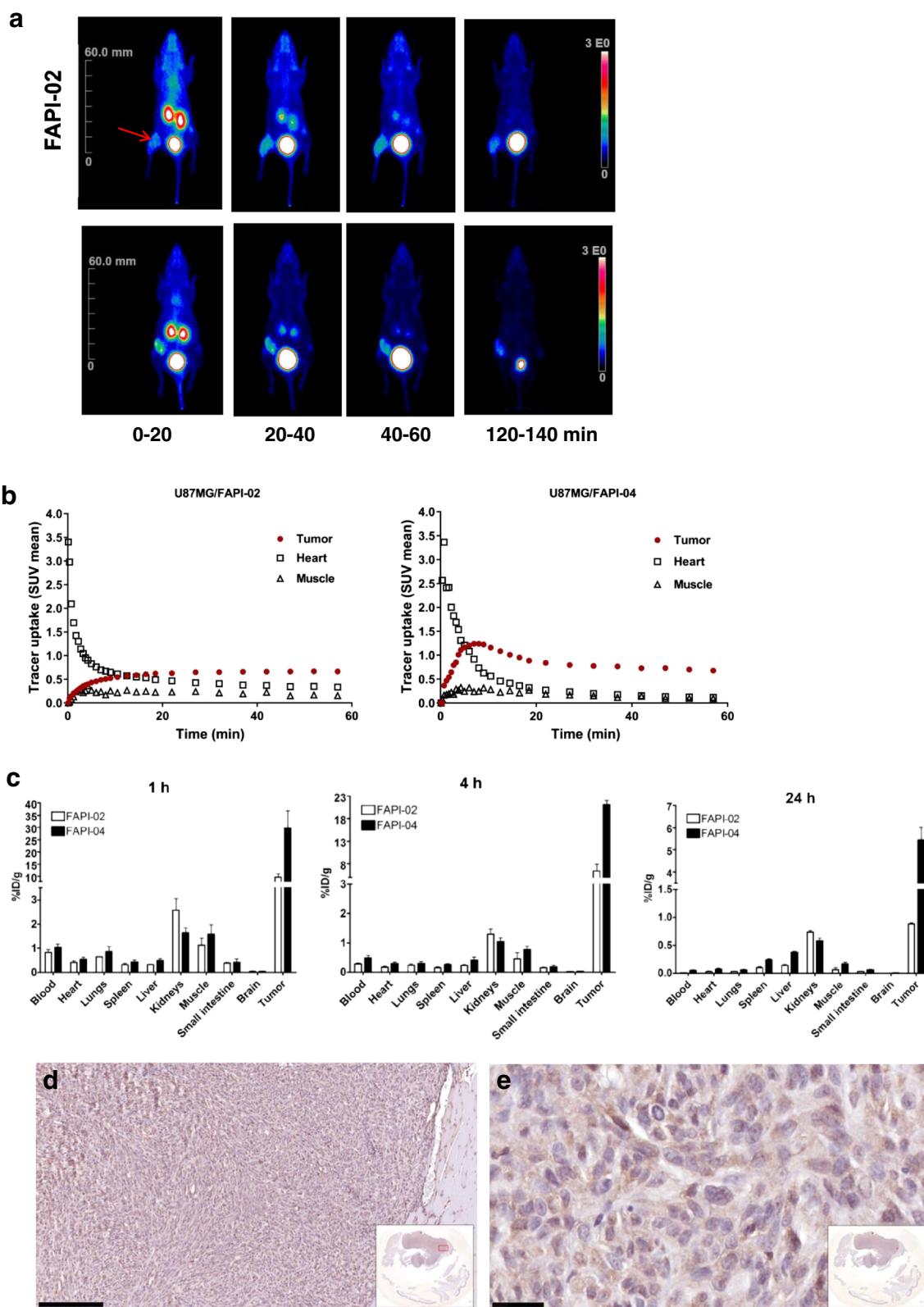
Fig. 1 **a** Exemplary images of small-animal PET of ^{68}Ga-labeled FAPI-02 and FAPI-04 in U87MG tumor–bearing nude mice up to 140 min after intravenous administration of the radiotracer. The tumors are indicated by the red arrows. **b** Corresponding time activity curves of FAPI-02 and FAPI-04 uptake in heart, muscle, and U87MG tumors. **c** Biodistribution of ^{177}Lu-labeled FAPI-02 and FAPI-04 in U87MG tumor–bearing nude mice 1, 4, and 24 h after intravenous administration of the radiotracers; $n = 3$. **d** FAP immunohistochemistry of subcutaneous xenograft tumors shows FAP positivity in variable extend within the tumors. **e** FAP-positive cells in a strongly FAP-positive area. Scale bars 250 μm (**d**) and 25 μm (**e**)
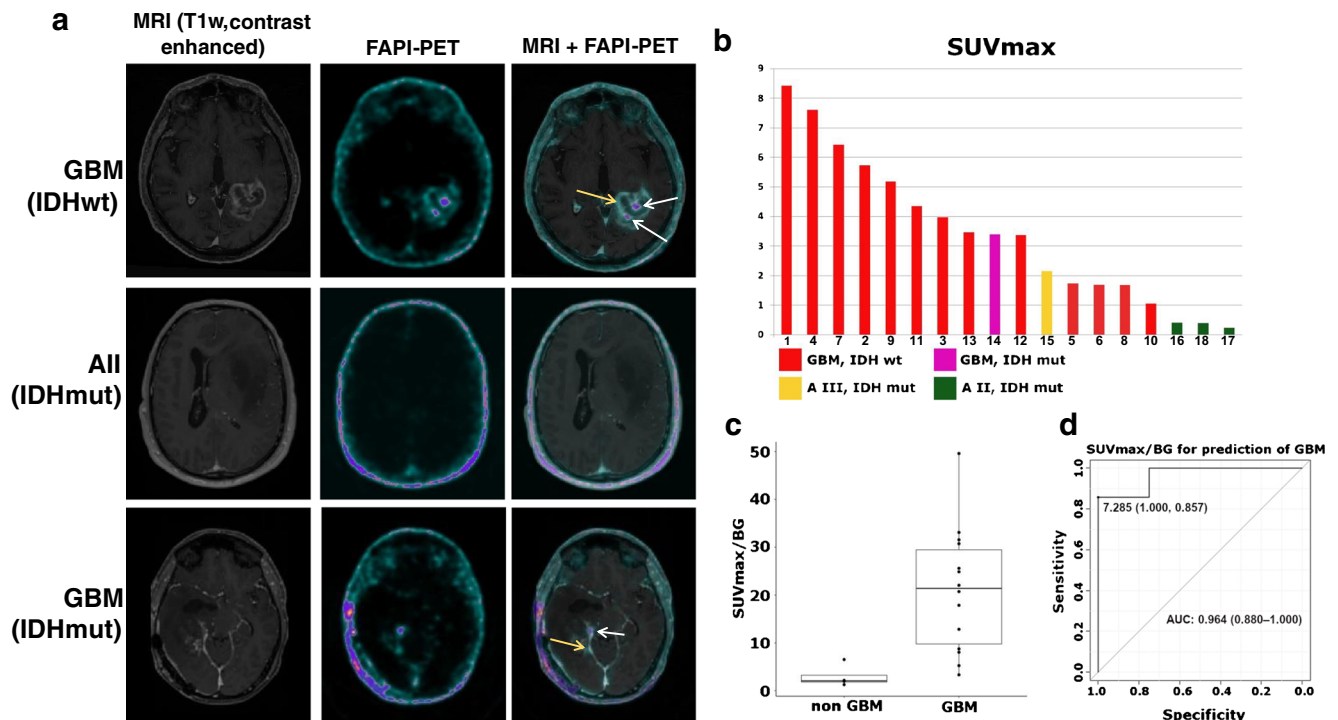
Fig. 2 **a** Exemplary images (contrast-enhanced T1-weighted MRI, FAP-specific PET using FAPI-04 and fused images of both modalities) of an IDH-wildtype glioblastoma (GBM (IDHwt)), an IDH-mutant astrocytoma WHO grade II (AII (IDHmut)) and an IDH-mutant glioblastoma (GBM (IDHmut)). The IDH-wildtype glioblastoma and the IDH-mutant glioblastoma both show foci with markedly increased tracer uptake (white arrows) within the contrast-enhancing lesion next to contrast-enhancing areas with only moderately elevated tracer uptake (yellow arrow). The IDH-mutant astrocytoma shows no elevated tracer uptake. **b** Absolute SUVmax values of all 18 gliomas. Patient numbers under each bar correspond with the patient numbers provided in Table 1 and the supplementary table. **c–h** Statistical analysis of SUVmax/BG values. **c–h** Boxplots of SUVmax/BG values and corresponding ROC curves in GBM versus non-GBM (**c**, **d**), IDH-mutant versus IDH-wildtype gliomas (**e**, **f**), and gliomas grade II versus gliomas grade III/IV (**g**, **h**)

between other cells (Fig. 3b–d). Second, we observed FAP-positive cells around the tumor vessels (Fig. 3c–f). Exemplary immunofluorescent co-stainings on a glioblastoma revealed that while FAP-positive cells were GFAP-negative, some co-expressed vimentin (Supplementary fig. 3a,b). FAP-positive cells occasionally showed mitoses (Supplementary fig. 3c). In an IDH-mutant anaplastic astrocytoma, perivascular FAP-positive cells were weakly positive for IDH1 R132H (Supplementary fig. 3d).

Discussion

Preclinical data

As demonstrated in previous publications, FAPI-02 and FAPI-04 exhibit specific FAP binding which can be completely reversed in competition experiments both in vitro and in vivo [7, 8]. Accordingly, no binding is observed to U87MG cells in vitro due to missing endogenous FAP expression. In vivo, however, both radiotracers show robust tumor accumulation in U87MG tumor xenografts. This observation is based on the recruitment and activation of mouse fibroblasts

and resulting FAPI binding to murine FAP expressed on these CAFs. On the other hand, FAP immunohistochemistry showed variably FAP-positive cells in xenograft tumors. This indicates that the initially FAP-negative tumor cells may become FAP-positive when exposed to in vivo conditions with crosstalk to environmental cells, such as CAFs. Both radiotracers accumulate quickly in the tumor but show rapid cell efflux at the same time, suggesting high cellular turnover. To gain more detailed insights regarding cellular kinetics and metabolism of the FAPI compounds, additional experiments are currently being performed.

Diagnostic accuracy

Next to morphological imaging, amino acid–based PET imaging (using FET, MET, or FDOPA) can be used for the imaging of cerebral gliomas [12, 14], whereas especially dynamic FET-PET has become a clinically well-established modality for the assessment of cerebral gliomas [10, 22]. A general criterion for the quality of diagnostic imaging of gliomas is the accuracy of non-invasive grading based on imaging parameters. The diagnostic accuracy of FET-PET parameters has frequently been evaluated over the last 15 years [23–26] and
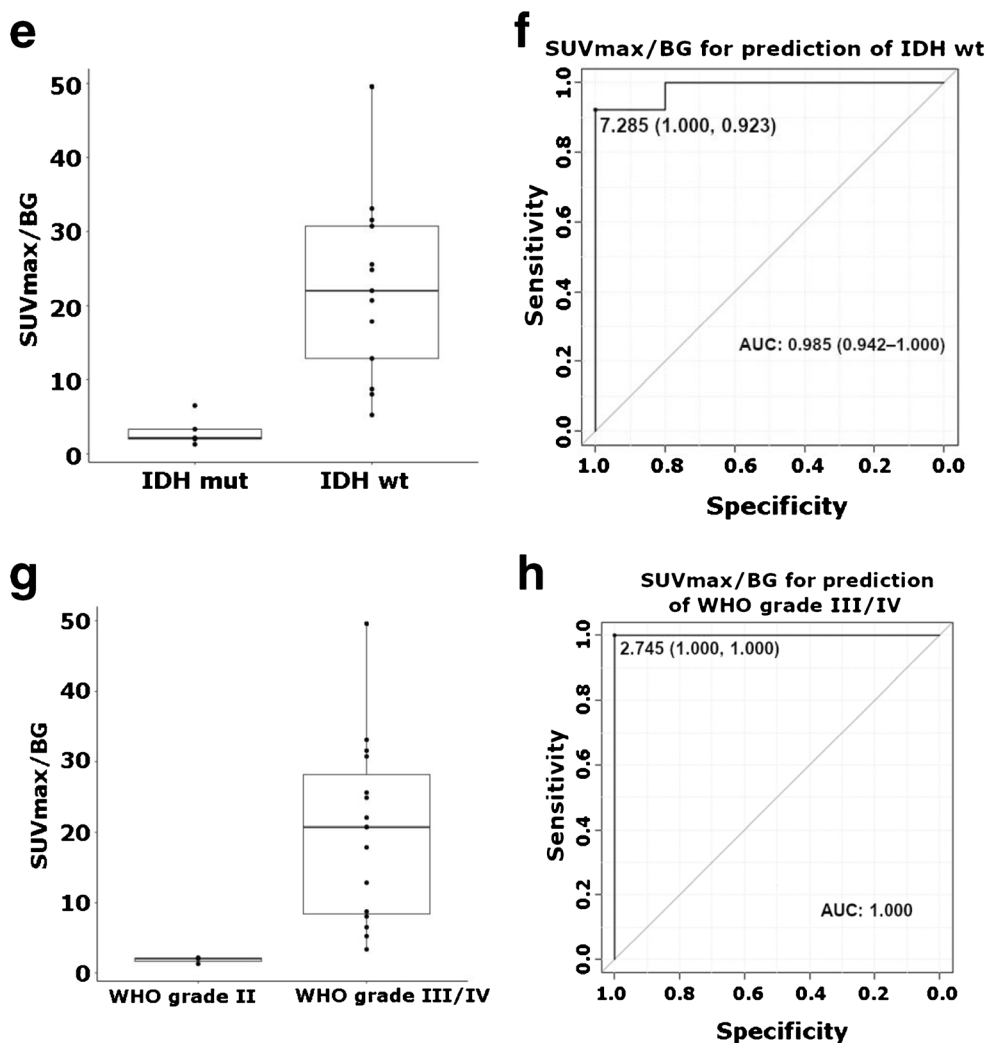
Fig. 2 (continued)

re-evaluated since the revised WHO classification of brain tumors 2016, in which the role of IDH mutation status for gliomas has been pointed out. In this study, the SUVmax/BG values showed high sensitivity and specificity for the prediction of WHO grade and IDH mutation status of the gliomas in our dataset. Especially, the AUC for the prediction of IDH mutation status (0.985) was markedly higher than the corresponding AUCs computed in two recent studies on dynamic FET-PET, in which single and combined dynamic parameters were analyzed (AUC 0.68–0.75 and 0.7–0.82) [27, 28]. Our results regarding tumor grading and prediction of IDH status must be considered preliminary due to the low total patient number and the unequal distribution of gliomas of different grades and IDH status. It must be pointed out that our dataset contained 13 IDH-wildtype glioblastomas WHO grade IV and three IDH-mutant gliomas, but no lower grade IDH-wildtype gliomas and only two IDH-mutant gliomas of WHO grade III/IV. Similarly, the two cited studies on FET-PET contained

predominantly IDH-mutant gliomas of WHO grade II and III. Thus, it is not clear if the prediction of IDH mutation status by FAP-specific or FET-PET imaging is WHO grade-independent or not. To further compare the diagnostic accuracy of FET-PET and FAP-targeted PET, studies with larger cohorts and head-to-head comparison of both tracers are needed.

Malignant progression of IDH-mutant tumors

IDH-mutant gliomas usually show a malignant transformation from WHO grade II to grade III or IV over time, whereas the clinical course of these tumors is extremely heterogeneous [9, 29, 30]. This fact is crucial for the monitoring of IDH-mutant gliomas of WHO grade II and III as the detection of malignant transformation has severe therapeutic consequences. The classical sign of malignant transformation is newly apparent contrast enhancement in T1w MRI due to breakdown of the

Fig. 3 **a** H&E of an area of a glioblastoma which immunohistochemically showed a strong FAP expression. **b–e** In many areas, spindle cells strongly stained for FAP (**b**, **c** higher magnification in **d**). However, also cells surrounding blood vessels were FAP-positive (**c**, higher magnification in **e**). In a different glioblastoma, primarily cells around microvascular proliferate stained for FAP (**f**). Scale bars 100 μm in a for **a–c**, 50 μm in **d** for **d–f**
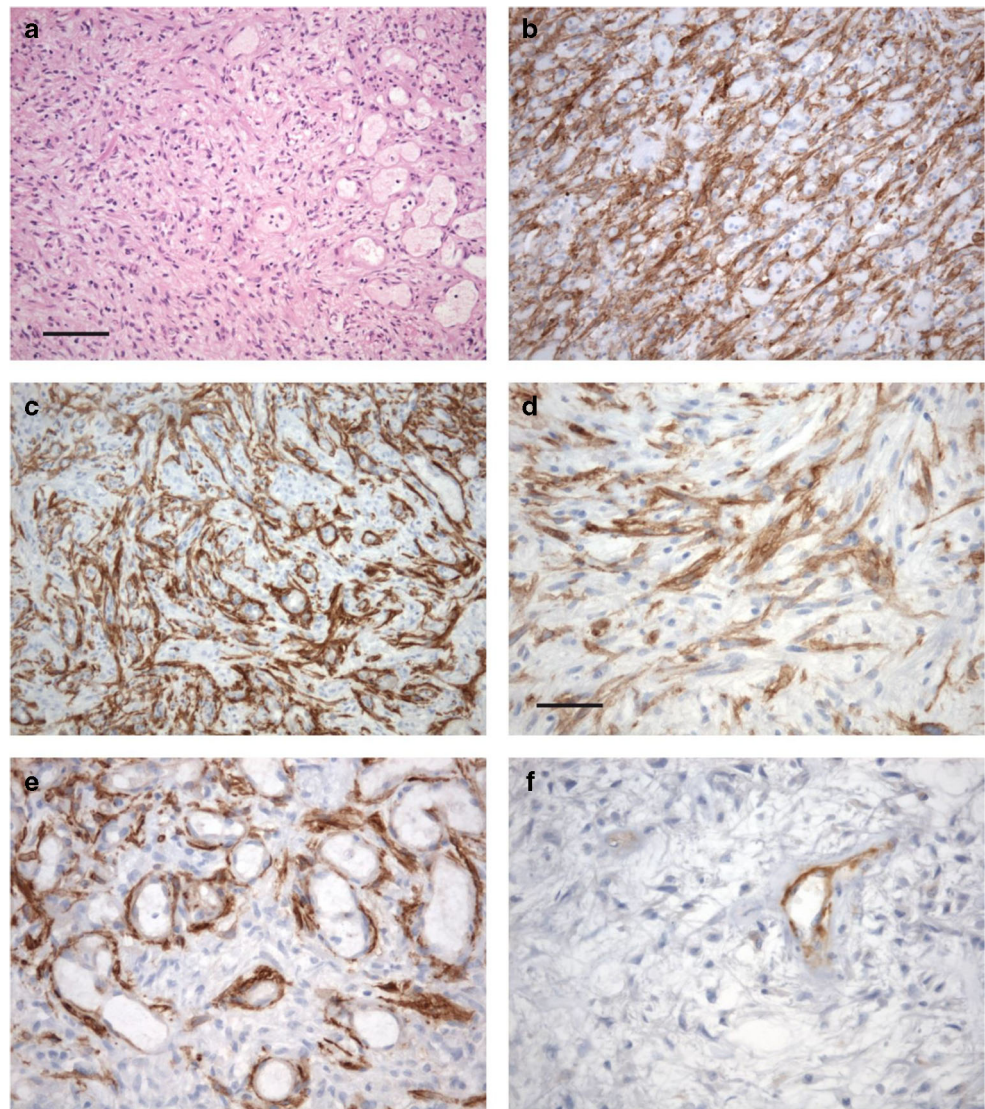
blood-brain barrier [31]. However, other, more subtle changes may precede contrast enhancement and great efforts have been made to detect these by additional imaging parameters. There is growing evidence that multiparametric MRI (reviewed in [32]) as well as PET imaging using FET or 2-deoxy-2-(18F) fluoro-D-glucose (FDG) may be helpful to identify patients with initially high risk of malignization [33, 34] and to detect malignant transformation of gliomas WHO grade II during follow-up [35–38], [17, 18, 39]. However, there is no consensus if and how PET imaging should be implemented into monitoring of initially WHO grade II IDH-mutant gliomas [32]. In our study, we observed a striking difference between the FAP-specific tracer uptake of IDH-mutant WHO grade II gliomas and grade III/IV gliomas. This finding makes it tempting to speculate that FAP positivity may be a predictor of malignant progression of WHO grade II gliomas to higher tumor grades. However, our preliminary dataset cannot

provide any definite conclusions towards the value of FAP-specific imaging for the detection of malignant progression of grade II gliomas. We consider it promising to evaluate FAP-specific PET imaging in comparison with MRI and FET—or FDG PET/CT in that context.

FAP immunohistochemistry pattern

With respect to glioma biology, it is of interest whether FAP is expressed by neoplastic glioma cells and/or by surrounding microenvironmental cells. In our immunohistochemical studies, we found two types of FAP-positive cells: (1) spindle-shaped, fibroblast-like cells intermingled with FAP-negative cells and (2) perivascular cells. Positivity of the pro-angiogenic FAP in the tumor vasculature has been reported before for glioblastomas and other tumors [15, 40, 41] and is in line with our findings.

There are some reports on cancer-associated fibroblast-like stromal cells in gliomas with similar promalignant effects as CAFs have in epithelial cancers [42–44]. On the other hand, there are reports of FAP expression in neoplastic glial cells and co-expression of FAP and the glial marker glial fibrillary acidic protein [15, 16]. Exemplary immunofluorescent co-stainings on a glioblastoma revealed that while FAP-positive cells were GFAP-negative, some co-expressed vimentin. Negativity for GFAP and positivity for Ki-67 and vimentin may support two different interpretations: FAP-positive cells could either be proliferating fibroblast-like stromal cells or de-differentiated neoplastic cells that have lost GFAP positivity during their de-differentiation. However, based on the small number of samples, we cannot make any definite conclusions about the biology of FAP-positive cells. Additional studies with larger number of cases may further define the nature of the FAP-positive cells.

Limitations of the study

The major limitation of this study is that all tumors, which were negative for FAP-specific PET, did not show contrast enhancement and all FAP-positive tumors showed contrast enhancement in the corresponding MRI. Thus, one cannot conclude from our data if tracer uptake in gliomas without breakdown of the blood-brain barrier is possible or not. Studies addressed to non-enhancing gliomas—analogous to existing studies for FET imaging—are necessary to answer this question and to evaluate the biological significance of FAP-specific PET in this group of gliomas. Similarly, it remains unclear if the inhomogeneous uptake pattern in grade III/IV gliomas reflects intratumoral differences of FAP expression or local inhomogeneity of tumor perfusion. An analysis of multiparametric MRI including perfusion and diffusion parameters and FAPI-PET/CT imaging parameters is currently underway which may address the potential correlation of FAP-positive foci in PET scans with perfusion hotspots. Another limitation of our clinical studies is that 5/18 patients have undergone pretreatments (radiotherapy or radiochemotherapy) before imaging. To evaluate possible treatment-associated changes in FAP-specific imaging, future studies are necessary.

Conclusion

In this pilot study, we retrospectively evaluated FAP-specific PET imaging in 18 gliomas. We observed focally increased tracer uptake in IDH-wildtype glioblastomas and WHO grade III/IV IDH-mutant astrocytomas. In contrast, WHO grade II astrocytomas did not show elevated tracer uptake. FAP-specific PET imaging may be of future relevance for non-invasive distinction between low-grade and high-grade gliomas and detection of malignant transformation of gliomas. FAP-specific PET imaging is a promising new technique for the assessment of gliomas but needs further evaluation in distinct clinical contexts and with a higher number of patients to re-examine the hypotheses that are generated by our work.

Compliance with ethical standards

References

1. Liao Z, Tan ZW, Zhu P, Tan NS. Cancer-associated fibroblasts in tumor microenvironment - accomplices in tumor malignancy. Cell Immunol. 2018. https://doi.org/10.1016/j.cellimm.2017.12.003.

2. Santi A, Kugeratski FG, Zanivan S. Cancer associated fibroblasts: the architects of stroma remodeling. Proteomics. 2018;18: e1700167. https://doi.org/10.1002/pmic.201700167.

3. Kalluri R. The biology and function of fibroblasts in cancer. Nat Rev Cancer. 2016;16:582–98. https://doi.org/10.1038/nrc.2016.73.

4. McCarthy JB, El-Ashry D, Turley EA. Hyaluronan, cancer-associated fibroblasts and the tumor microenvironment in malignant progression. Front Cell Dev Biol. 2018;6:48. https://doi.org/10.3389/fcell.2018.00048.

5. Lai D, Ma L, Wang F. Fibroblast activation protein regulates tumor-associated fibroblasts and epithelial ovarian cancer cells. Int J Oncol. 2012;41:541–50. https://doi.org/10.3892/ijo.2012.1475.

6. Koczorowska MM, Tholen S, Bucher F, Lutz L, Kizhakkedathu JN, De Wever O, et al. Fibroblast activation protein-alpha, a stromal cell surface protease, shapes key features of cancer associated fibroblasts through proteome and degradome alterations. Mol Oncol. 2016;10:40–58. https://doi.org/10.1016/j.molonc.2015.08.001.

7. Loktev A, Lindner T, Mier W, Debus J, Altmann A, Jager D, et al. A new method for tumor imaging by targeting cancer associated fibroblasts. J Nucl Med. 2018. https://doi.org/10.2967/jnumed.118.210435.

8. Lindner T, Loktev A, Altmann A, Giesel F, Kratochwil C, Debus J, et al. Development of quinoline based theranostic ligands for the

targeting of fibroblast activation protein. J Nucl Med. 2018. https://doi.org/10.2967/jnumed.118.210443.

9. Louis DN, Perry A, Reifenberger G, von Deimling A, Figarella-Branger D, Cavenee WK, et al. The 2016 World Health Organization classification of tumors of the central nervous system: a summary. Acta Neuropathol. 2016;131:803–20. https://doi.org/10.1007/s00401-016-1545-1.

10. Langen KJ, Stoffels G, Filss C, Heinzel A, Stegmayr C, Lohmann P, et al. Imaging of amino acid transport in brain tumours: positron emission tomography with O-(2-[(18)F]fluoroethyl)-L-tyrosine (FET). Methods. 2017;130:124–34. https://doi.org/10.1016/j.ymeth.2017.05.019.

11. Palanichamy K, Chakravarti A. Diagnostic and prognostic significance of methionine uptake and methionine positron emission tomography imaging in gliomas. Front Oncol. 2017;7:257. https://doi.org/10.3389/fonc.2017.00257.

12. Hoffman RM. L-[methyl-(11)C] Methionine-positron-emission tomography (MET-PET). Methods Mol Biol. 1866;2019:267–71. https://doi.org/10.1007/978-1-4939-8796-2_20.

13. Bell C, Dowson N, Puttick S, Gal Y, Thomas P, Fay M, et al. Increasing feasibility and utility of (18)F-FDOPA PET for the management of glioma. Nucl Med Biol. 2015;42:788–95. https://doi.org/10.1016/j.nucmedbio.2015.06.001.

14. Fueger BJ, Czernin J, Cloughesy T, Silverman DH, Geist CL, Walter MA, et al. Correlation of 6-18F-fluoro-L-dopa PET uptake with proliferation and tumor grade in newly diagnosed and recurrent gliomas. J Nucl Med. 2010;51:1532–8. https://doi.org/10.2967/jnumed.110.078592.

15. Busek P, Balaziova E, Matrasova I, Hilser M, Tomas R, Syrucek M, et al. Fibroblast activation protein alpha is expressed by transformed and stromal cells and is associated with mesenchymal features in glioblastoma. Tumour Biol. 2016;37:13961–71. https://doi.org/10.1007/s13277-016-5274-9.

16. Mentlein R, Hattermann K, Hemion C, Jungbluth AA, Held-Feindt J. Expression and role of the cell surface protease seprase/fibroblast activation protein-alpha (FAP-alpha) in astroglial tumors. Biol Chem. 2011;392:199–207. https://doi.org/10.1515/BC.2010.119.

17. Floca R. MatchPoint: on bridging the innovation gap between algorithmic research and clinical use in image registration. World Congress on Medical Physics and Biomedical Engineering, September 7–12, 2009, Munich, Germany. 2009:1105–8.

18. Nolden M, Zelzer S, Seitel A, Wald D, Muller M, Franz AM, et al. The medical imaging interaction toolkit: challenges and advances : 10 years of open-source development. Int J Comput Assist Radiol Surg. 2013;8:607–20. https://doi.org/10.1007/s11548-013-0840-8.

19. RCoreTeam. R: A language and environment for statistical computing. R Foundation for Statistical Computing. 2017.

20. Robin X, Turck N, Hainard A, Tiberti N, Lisacek F, Sanchez J-C, et al. pROC: an open-source package for R and S+ to analyze and compare ROC curves. BMC Bioinformatics. 2011;12:1.

21. Kelly T. Fibroblast activation protein-alpha and dipeptidyl peptidase IV (CD26): cell-surface proteases that activate cell signaling and are potential targets for cancer therapy. Drug Resist Updat. 2005;8:51–8. https://doi.org/10.1016/j.drup.2005.03.002.

22. Albert NL, Weller M, Suchorska B, Galldiks N, Soffietti R, Kim MM, et al. Response Assessment in Neuro-Oncology working group and European Association for Neuro-Oncology recommendations for the clinical use of PET imaging in gliomas. Neuro-Oncology. 2016;18:1199–208. https://doi.org/10.1093/neuonc/now058.

23. Albert NL, Winkelmann I, Suchorska B, Wenter V, Schmid-Tannwald C, Mille E, et al. Early static (18)F-FET-PET scans have a higher accuracy for glioma grading than the standard 20-40 min scans. Eur J Nucl Med Mol Imaging. 2016;43:1105–14. https://doi.org/10.1007/s00259-015-3276-2.

24. Jansen NL, Graute V, Armbruster L, Suchorska B, Lutz J, Eigenbrod S, et al. MRI-suspected low-grade glioma: is there a need to perform dynamic FET PET? Eur J Nucl Med Mol Imaging. 2012;39:1021–9. https://doi.org/10.1007/s00259-012-2109-9.

25. Pauleit D, Floeth F, Hamacher K, Riemenschneider MJ, Reifenberger G, Muller HW, et al. O-(2-[18F]fluoroethyl)-L-tyrosine PET combined with MRI improves the diagnostic assessment of cerebral gliomas. Brain. 2005;128:678–87. https://doi.org/10.1093/brain/awh399.

26. Popperl G, Kreth FW, Mehrkens JH, Herms J, Seelos K, Koch W, et al. FET PET for the evaluation of untreated gliomas: correlation of FET uptake and uptake kinetics with tumour grading. Eur J Nucl Med Mol Imaging. 2007;34:1933–42. https://doi.org/10.1007/s00259-007-0534-y.

27. Rohrich M, Huang K, Schrimpf D, Albert NL, Hielscher T, von Deimling A, et al. Integrated analysis of dynamic FET PET/CT parameters, histology, and methylation profiling of 44 gliomas. Eur J Nucl Med Mol Imaging. 2018;45:1573–84. https://doi.org/10.1007/s00259-018-4009-0.

28. Verger A, Stoffels G, Bauer EK, Lohmann P, Blau T, Fink GR, et al. Static and dynamic (18)F-FET PET for the characterization of gliomas defined by IDH and 1p/19q status. Eur J Nucl Med Mol Imaging. 2018;45:443–51. https://doi.org/10.1007/s00259-017-3846-6.

29. Di Carlo DT, Duffau H, Cagnazzo F, Benedetto N, Morganti R, Perrini P. IDH wild-type WHO grade II diffuse low-grade gliomas. A heterogeneous family with different outcomes. Systematic review and meta-analysis. Neurosurg Rev. 2018. https://doi.org/10.1007/s10143-018-0996-3.

30. Reuss DE, Mamatjan Y, Schrimpf D, Capper D, Hovestadt V, Kratz A, et al. IDH mutant diffuse and anaplastic astrocytomas have similar age at presentation and little difference in survival: a grading problem for WHO. Acta Neuropathol. 2015;129:867–73. https://doi.org/10.1007/s00401-015-1438-8.

31. Pallud J, Capelle L, Taillandier L, Fontaine D, Mandonnet E, Guillevin R, et al. Prognostic significance of imaging contrast enhancement for WHO grade II gliomas. Neuro-Oncology. 2009;11:176–82. https://doi.org/10.1215/15228517-2008-066.

32. Freyschlag CF, Krieg SM, Kerschbaumer J, Pinggera D, Forster MT, Cordier D, et al. Imaging practice in low-grade gliomas among European specialized centers and proposal for a minimum core of imaging. J Neuro-Oncol. 2018;139:699–711. https://doi.org/10.1007/s11060-018-2916-3.

33. Gempt J, Bette S, Ryang YM, Buchmann N, Peschke P, Pyka T, et al. 18F-Fluoro-ethyl-tyrosine positron emission tomography for grading and estimation of prognosis in patients with intracranial gliomas. Eur J Radiol. 2015;84:955–62. https://doi.org/10.1016/j.ejrad.2015.01.022.

34. Jansen NL, Suchorska B, Wenter V, Eigenbrod S, Schmid-Tannwald C, Zwergal A, et al. Dynamic 18F-FET PET in newly diagnosed astrocytic low-grade glioma identifies high-risk patients. J Nucl Med. 2014;55:198–203. https://doi.org/10.2967/jnumed.113.122333.

35. Unterrainer M, Schweisthal F, Suchorska B, Wenter V, Schmid-Tannwald C, Fendler WP, et al. Serial 18F-FET PET imaging of primarily 18F-FET-negative glioma: does it make sense? J Nucl Med. 2016;57:1177–82. https://doi.org/10.2967/jnumed.115.171033.

36. Imani F, Boada FE, Lieberman FS, Davis DK, Deeb EL, Mountz JM. Comparison of proton magnetic resonance spectroscopy with fluorine-18 2-fluoro-deoxyglucose positron emission tomography for assessment of brain tumor progression. J Neuroimaging. 2012;22:184–90. https://doi.org/10.1111/j.1552-6569.2010.00561.x.

37. Dankbaar JW, Snijders TJ, Robe PA, Seute T, Eppinga W, Hendrikse J, et al. The use of (18)F-FDG PET to differentiate

progressive disease from treatment induced necrosis in high grade glioma. J Neuro-Oncol. 2015;125:167–75. https://doi.org/10.1007/s11060-015-1883-1.

38. Henze M, Mohammed A, Schlemmer HP, Herfarth KK, Hoffner S, Haufe S, et al. PET and SPECT for detection of tumor progression in irradiated low-grade astrocytoma: a receiver-operating-characteristic analysis. J Nucl Med. 2004;45:579–86.

39. Capper D, Zentgraf H, Balss J, Hartmann C, von Deimling A. Monoclonal antibody specific for IDH1 R132H mutation. Acta Neuropathol. 2009;118:599–601. https://doi.org/10.1007/s00401-009-0595-z.

40. Hamson EJ, Keane FM, Tholen S, Schilling O, Gorrell MD. Understanding fibroblast activation protein (FAP): substrates, activities, expression and targeting for cancer therapy. Proteomics Clin Appl. 2014;8:454–63. https://doi.org/10.1002/prca.201300095.

41. Aimes RT, Zijlstra A, Hooper JD, Ogbourne SM, Sit ML, Fuchs S, et al. Endothelial cell serine proteases expressed during vascular morphogenesis and angiogenesis. Thromb Haemost. 2003;89:561–72.

42. Clavreul A, Etcheverry A, Chassevent A, Quillien V, Avril T, Jourdan ML, et al. Isolation of a new cell population in the glioblastoma microenvironment. J Neuro-Oncol. 2012;106:493–504. https://doi.org/10.1007/s11060-011-0701-7.

43. Clavreul A, Guette C, Faguer R, Tetaud C, Boissard A, Lemaire L, et al. Glioblastoma-associated stromal cells (GASCs) from histologically normal surgical margins have a myofibroblast phenotype and angiogenic properties. J Pathol. 2014;233:74–88. https://doi.org/10.1002/path.4332.

44. Trylcova J, Busek P, Smetana K Jr, Balaziova E, Dvorankova B, Mifkova A, et al. Effect of cancer-associated fibroblasts on the migration of glioma cells in vitro. Tumour Biol. 2015;36:5873–9. https://doi.org/10.1007/s13277-015-3259-8.